Pattern Recognition 43 (2010) 2833–2844

Contents lists available at ScienceDirect

Pattern Recognition

journal homepage: www.elsevier.com/locate/pr

Adaptive fingerprint pore modeling and extraction ☆

Qijun Zhao, David Zhang *, Lei Zhang, Nan Luo

Biometrics Research Centre, Department of Computing, The Hong Kong Polytechnic University, Hung Hom, Kowloon, Hong Kong

ARTICLE INFO

Article history:
Received 30 October 2009
Received in revised form
15 December 2009
Accepted 20 February 2010

Keywords:
Automatic fingerprint recognition
Pore extraction
Pore models
Biometrics

ABSTRACT

Sweat pores on fingerprints have proven to be discriminative features and have recently been successfully employed in automatic fingerprint recognition systems (AFRS), where the extraction of fingerprint pores is a critical step. Most of the existing pore extraction methods detect pores by using a static isotropic pore model; however, their detection accuracy is not satisfactory due to the limited approximation capability of static isotropic models to various types of pores. This paper presents a dynamic anisotropic pore model to describe pores more accurately by using orientation and scale parameters. An adaptive pore extraction method is then developed based on the proposed dynamic anisotropic pore model. The fingerprint image is first partitioned into well-defined, ill-posed, and background blocks. According to the dominant ridge orientation and frequency on each foreground block, a local instantiation of appropriate pore model is obtained. Finally, the pores are extracted by filtering the block with the adaptively generated pore model. Extensive experiments are performed on the high resolution fingerprint databases we established. The results demonstrate that the proposed method can detect pores more accurately and robustly, and consequently improve the fingerprint recognition accuracy of pore-based AFRS.

1. Introduction

Fingerprint is the most widely used biometric characteristic for personal identification because of its uniqueness and stability over time [1–3]. Most of the existing automatic fingerprint recognition systems (AFRS) use the minutia features on fingerprints, i.e. the terminations and bifurcations of fingerprint ridges [4,14,23], for recognition. Although they can achieve good recognition accuracy and have been used in many civil applications, their performance still needs much improvement when a large population is involved or a high security level is required. One solution to enhancing the accuracy of AFRS is to employ more features on fingerprints other than only minutiae [11,22,24].

Generally, fingerprint features can be divided into three levels [5]. Level 1 features (e.g. overall fingerprint ridge patterns) and Level 2 features (e.g. minutiae) have been extensively studied and they are employed in most existing AFRS. Level 3 features, however, are ignored in many AFRS even though they are also very distinctive and have been used for a long time in the forensic community [15,16]. Level 3 features refer to ridge dimensional attributes such as ridge contours and pores, which are fine details on ridges and require high resolution imaging techniques to reliably capture [5]. Such requirements limit the use of Level 3 features in conventional AFRS. Thanks to the advances in imaging techniques and the demand for more secure biometric systems, recently researchers have been paying more and more attention to using Level 3 features in AFRS. Roddy and Stosz [6], and Parsons et al. [13] statistically analyzed the discriminative power of pores and validated the effectiveness of pore configuration in personal identification. The first AFRS using pores was developed by Stosz and Alyea [7]. They combined minutiae and pores to recognize persons. Subsequently, Kryszczuk et al. [8,9] investigated the contribution of pores to fragmentary fingerprint recognition and showed that the smaller the fingerprint fragments, the greater the benefit of using pores. Recently, Jain et al. [10,11] proposed a high resolution fingerprint recognition system which uses features from all the three levels (i.e. ridge orientation fields, minutiae, ridge contours, and pores).

A critical step in the pore based AFRS is the extraction of pores from fingerprint images. Existing methods extract pores by using skeleton-tracking-based [6–9] or filtering-based approaches [10–13]. The skeleton-tracking-based approaches are quite time-consuming and work well only with very high quality fingerprint images [10,11]. The filtering-based approaches are more efficient and more robust. They use static isotropic pore models to detect pores. As we will see later, however, the pores on real fingerprint images appear anisotropic and vary greatly in scale from fingerprint to fingerprint and from region to region.

In this paper we will first propose a novel dynamic anisotropic pore model which describes the pores more flexibly and accurately than the previous models. With the proposed pore model,

☆ A preliminary version of this paper was presented on the 19th International Conference on Pattern Recognition (ICPR2008).

* Corresponding author. Tel.: +852 27667271; fax: +852 27740842.
E-mail addresses: csqjzhao@comp.polyu.edu.hk, csdzhang@comp.polyu.edu.hk (D. Zhang).

0031-3203/$ - see front matter © 2010 Elsevier Ltd. All rights reserved.
doi:10.1016/j.patcog.2010.02.016

we will then develop an adaptive pore extraction method to accurately and robustly extract pores. To evaluate the proposed method, we established two sets of high resolution fingerprint images and conducted extensive experiments on them. The results demonstrated that the proposed pore model and pore extraction method can detect pores more accurately and robustly than the previous methods, and the extracted pore features can consequently improve the recognition accuracy of pore based AFRS.

The rest of the paper is organized as follows. Section 2 reviews the existing pore models and the pore extraction methods. Section 3 introduces the proposed dynamic anisotropic pore model. Section 4 presents the adaptive pore extraction method in detail. Section 5 performs extensive experiments on pore extraction and recognition by using the established high resolution fingerprint databases. Section 6 concludes the paper.

2. Review of existing pore extraction methods

Existing pore extraction methods can be classified into two categories, skeleton-tracking-based methods and filtering-based methods. All earlier works [6–9] are skeleton-tracking-based methods. They first binarize and skeletonize the fingerprint image and then track the fingerprint skeletons. A pore is detected when certain criteria are met during the tracking. As pointed out in [10,11], however, skeletonization is computationally expensive and very sensitive to noise and it works well only on very high resolution fingerprint images of high quality. For example, the fingerprint images used in [6–9] are all at least 2000dpi. Recently proposed approaches are filtering-based methods that detect pores by using pore models to filter fingerprint images. Fig. 1 shows three typical isotropic pore models: Ray's model [12], Jain's model [10,11], and the DoG (difference of Gaussian) model [13].

Ray et al. [12] proposed an approach to extracting pores from fingerprint images based on the pore model in Fig. 1(a), which is a modified 2-dimensional Gaussian function. They first calculated an error map for the fingerprint image, with each entry in this map being the sum of the squared errors between the pore model and the local area surrounding the pixel. The error map is then binarized such that only areas of high pore probability (i.e. low error) are retained. In these areas, the pores are detected as the local minima in a $(2r_m)\times(2r_m)$ neighborhood. In [12], the authors used unitary parameters r (the variance of the Gaussian) and r_m to detect pores. However, the pore scales and ridge/valley widths could vary greatly from one fingerprint to another fingerprint or from one region to another region in the same fingerprint (referring to Fig. 2 for examples). Moreover, Ray's pore model is isotropic, yet as we can see from Fig. 2 that the appearance of open pores on real fingerprint images is not isotropic.

More recently, Jain et al. [10,11] proposed to use the Mexican hat wavelet transform to extract pores based on the observation that pore regions typically have a high negative frequency response as intensity values change abruptly from bright to dark at the pores. The Mexican hat wavelet actually serves as the pore model, and its scale parameter is experimentally set for specific datasets. Fig. 1(b) shows the Mexican hat wavelet. Obviously, it is also isotropic. This pore model is also limited in that it cannot adapt itself to different fingerprints or different regions on a fingerprint.

Another pore extraction method was proposed by Parsons et al. [13]. Its basic idea is to use a band-pass filter to detect circle-like features. In other words, the method assumes that pores appear as circular objects on fingerprint images, and the pore is thus modeled by the DoG filter. Fig. 1(c) shows this pore model. In [13], the authors did not consider the variation of pore scales in fingerprint images but simply used a unitary scale in their model. To deal with the limitations caused by unitary scale, we have recently proposed in [25] an adaptive DoG-based pore extraction method. It divides a fingerprint image into blocks and defines for each block a DoG filter according to the local ridge period on the block. One limitation of the DoG-based methods is that the pore models are isotropic. The underlying assumption that pores are circular features does not hold well on real fingerprint images. In this paper, we will propose another novel pore model and extraction method, which can well solve the problems with existing pore models and extraction methods. Next, we introduce the new pore model first.

3. Dynamic anisotropic pore model (DAPM)

Sweat pores reside on finger ridges and may be either closed or open [15]. As can be seen in Fig. 2, a closed pore looks like an isolated bright blob on the dark ridge, whereas an open pore, which is perspiring, is connected with its neighboring bright valleys. To investigate the spatial appearances of pores on fingerprint images, we manually marked and cropped hundreds of pores on many fingerprint images, including both open and closed pores. We generalized three types of representative pore structures, which are illustrated in Fig. 3. It can be seen that the two open pores (b) and (c) are not isotropic. Along the ridge direction, all the three types of pores appear with Gaussian-shaped profiles. Furthermore, the width of Gaussian profile will vary from one pore to another.

These observations clearly show that the previously proposed pore models (refer to Section 2) are not accurate enough to model the various pores because they are isotropic and static (i.e. using a unitary scale). In order to represent the pores more accurately, we propose here a new pore model which has two parameters to adjust scale and orientation. When applying this model to a real pore, these two parameters are adaptively determined according to the local ridge features (i.e. ridge orientation and frequency). Therefore, we name the proposed model as the dynamic anisotropic pore model (DAPM), which is defined as follows:

$$\begin{cases} P_0(i,j) = e^{(-j^2/2\sigma^2)}\cos\left(\dfrac{\pi}{3\sigma}i\right) \\ -3\sigma \le i, \quad j \le 3\sigma \end{cases} \tag{1}$$

$$\begin{cases} P_\theta(i,j) = Rot(P_0,\theta) = e^{-(\hat{j}^2/2\sigma^2)}\cos\left(\dfrac{\pi}{3\sigma}\hat{i}\right) \\ \hat{i} = i\cos(\theta) - j\sin(\theta), \quad \hat{j} = i\sin(\theta) + j\cos(\theta) \\ -3\sigma \le i, \quad j \le 3\sigma \end{cases} \tag{2}$$

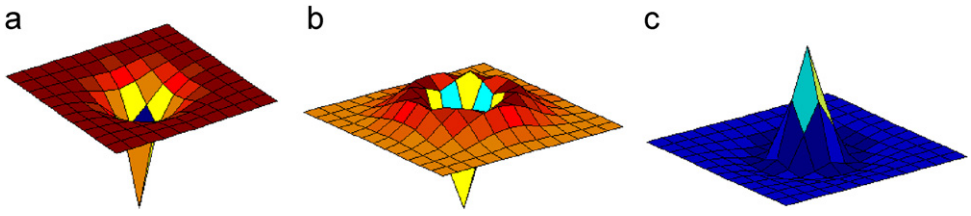

Fig. 1. Three typical pore models: (a) Ray's model [12], (b) Jain's model [10,11], and (c) the DoG model [13], which are all isotropic.

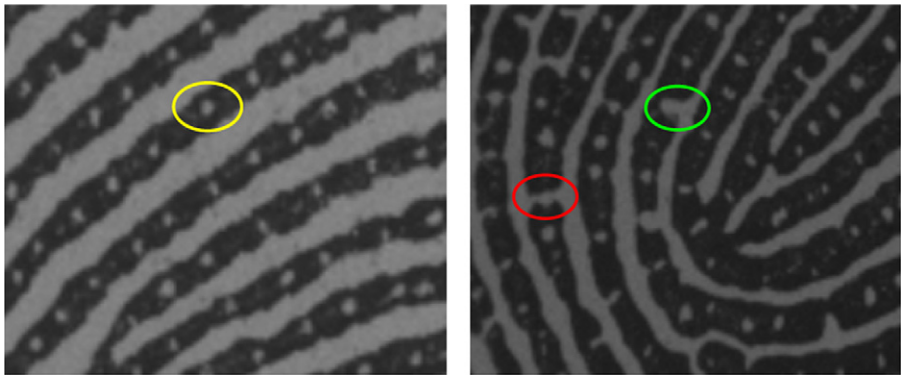

Fig. 2. Two fingerprint images with very different ridge and valley widths. A closed pore is marked on the left image and two open pores are marked on the right image.

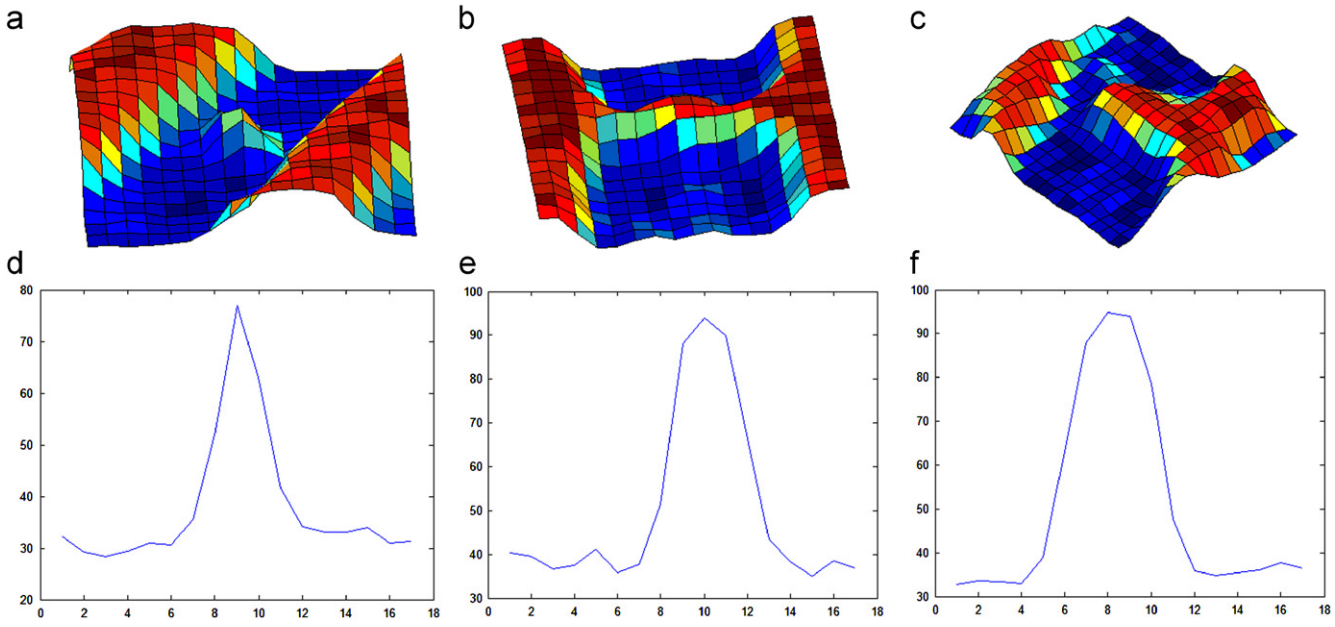

Fig. 3. The appearance of three typical pores on real fingerprint images. (a) is a closed pore, and (b) and (c) are open pores. (d)–(f) are the corresponding intensity profiles across them along the ridge orientation. All the profiles are Gaussian-shaped.

Eq. (1) is the reference model (i.e. the zero-degree model) and Eq. (2) is the rotated model. Here, σ is the scale parameter which is used to control the pore size. It can be determined by the local ridge frequency. θ is the orientation parameter which is used to control the direction of the pore model. It can be estimated by the local ridge orientation. Fig. 4 shows some example instances of the proposed DAPM. With the proposed DAPM, next we present an adaptive pore extraction method in Section 4.

4. Adaptive pore extraction

Pore extraction is essentially a problem of object detection. Generally, given a model of an object, we can detect the object by using the model as a matched filter. When convoluting an image with a matched filter describing the desired object, strong responses will be obtained at the locations of the object on the image. The techniques of matched filters have been successfully used in many applications, for example, vessel detection on retinal images [17]. In this section, we will first estimate the parameters in the DAPM to instantiate the pore model, and then discuss the important implementation issues in using the instantiated pore models to extract pores. Finally, the adaptive pore extraction algorithm will be presented.

4.1. DAPM parameter estimation

The matched filters for pore extraction can be generated by instantiating the pore models. In order to instantiate the DAPM in Eqs. (1) and (2), it is necessary to initialize two parameters, orientation θ and scale σ. As for the orientation parameter θ, an intuitive way is to set it as the local fingerprint ridge orientation. To estimate the ridge orientation field on the fingerprint, we first smooth the fingerprint image by using a smoothing kernel and then calculate the gradients along the x and y directions by using some derivative operator (e.g. the Sobel operator). Let $G_x(i,j)$ and $G_y(i,j)$ be the gradients at the pixel (i,j), and the squared gradients be $G_{xx}(i,j)=G_x(i,j)\times G_x(i,j)$, $G_{xy}(i,j)=G_x(i,j)\times G_y(i,j)$, and $G_{yy}(i,j)=G_y(i,j)\times G_y(i,j)$. The squared gradients are then smoothed by using a Gaussian kernel, resulting in $\overline{G}_{xx}$, $\overline{G}_{xy}$, and $\overline{G}_{yy}$. The ridge orientation

at (i,j) is estimated by

$$O(i,j)=\frac{\pi}{2}+\frac{1}{2}\bullet\arctan\left(\frac{\overline{G}_{xx}(i,j)-\overline{G}_{yy}(i,j)}{2\bullet\overline{G}_{xy}(i,j)}\right) \tag{3}$$

which is in the range of $[0,\pi]$. For more details on fingerprint ridge orientation field estimation, please refer to [18].

With regard to the scale parameter σ, if we can estimate the range of pore scales, we can then use a bank of multi-scale matched filters to detect the pores; however, this is very time-consuming. Therefore, we estimate and use the maximum valid pore scale when designing the matched filters in this paper. As shown in Section 2, the pores are located on ridges. Consequently, the pore scales should be restricted by the ridge widths. This motivates us to associate the maximum pore scale with the local fingerprint ridge period by a ratio, i.e. $\sigma=\tau/k$, where τ is the local ridge period (or the reciprocal of local ridge frequency) and k a positive constant. In this paper, we empirically set $k=12$. The local ridge frequency is estimated in a local window by using the projection-based method in [19].

4.2. Implementation issues

With the estimated parameters θ and σ in Section 4.1, an adaptive pore model can be instantiated for each pixel and then we can apply it as a matched filter to extracting pores from the fingerprint image. However, there will be two problems if directly applying the matched filters in a pixel-wise way. Next, we discuss these issues in detail and present the solutions to practical implementation.

The first problem is the computational cost. Obviously, it will be very expensive to calculate the DAPM in a pixel-wise way. Noting that in a local region on the fingerprint, the ridges run nearly parallel with each other, and the intervals between them vary slightly, we could therefore calculate a common DAPM in a local region to detect pores. The second problem is that on some parts of a fingerprint image it is difficult to get an accurate estimate of the local ridge orientation and frequency, which is needed in order to initialize an accurate instance of DAPM. For example, on the image shown in Fig. 5(a), the region highlighted by the red circle is mashed and no dominant orientation can be obtained. The sharp change of ridge orientation at the singular points of a fingerprint will also raise difficulties in estimating the ridge orientation and frequency surrounding the singular points.

To deal with these issues, we propose a block-wise approach to implementing the matched filters for pore extraction. This approach defines three kinds of blocks on fingerprint images: well-defined blocks, ill-posed blocks, and background blocks. Well-defined and ill-posed blocks are both foreground fingerprint regions. On a well-defined block, it is able to directly estimate a dominant ridge orientation and a ridge frequency. On an ill-posed block, there is not a dominant ridge orientation but the ridge frequency can be estimated by interpolation of the frequencies on its neighboring blocks.

The block partition and classification is performed in a hierarchical way. First, a large block size is applied to the image. For each block B, the following structure tensor is calculated

$$J=\frac{1}{N_B}\sum_{i\in B}\nabla B_i\nabla B_i^T=\begin{bmatrix}j_{11} & j_{12}\\ j_{21} & j_{22}\end{bmatrix} \tag{4}$$

where N_B denotes the number of pixels in the block, $\nabla B_i=((\partial B_i/\partial x),(\partial B_i/\partial y))^T$ is the gradient vector at pixel i, and 'T' represents the transpose operator. The structure tensor J contains information of ridge orientation in the block and the eigenvalues of J can be used to measure the consistency of ridge orientation. Specifically, we use the orientation certainty (OC) defined as follows [20]:

$$OC=\frac{(\lambda_1-\lambda_2)^2}{(\lambda_1+\lambda_2)^2}=\frac{(j_{11}-j_{22})^2+4j_{12}^2}{(j_{11}+j_{22})^2} \tag{5}$$

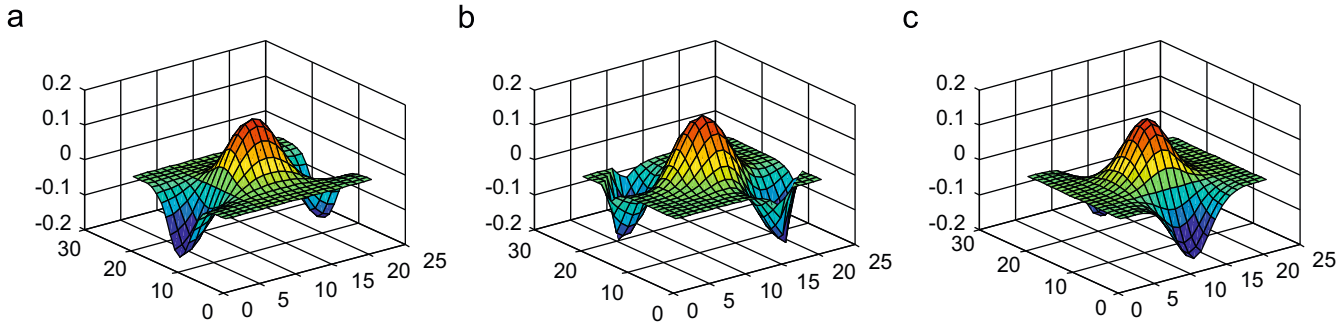

Fig. 4. Examples of the dynamic anisotropic pore model. (a) $\theta=0$, (b) $\theta=45$, and (c) $\theta=90$.

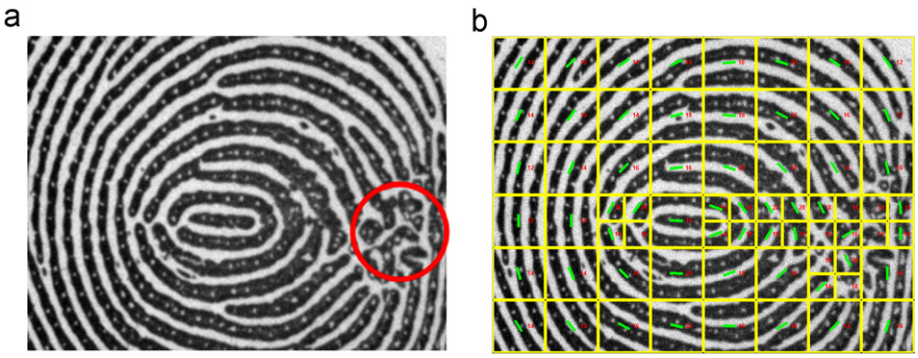

Fig. 5. (a) A fingerprint image. The ridge orientation and frequency cannot be accurately estimated on the region marked by the red circle. (b) The partition result. The dominant ridge orientations of the well-defined blocks are shown by the green lines. (For interpretation of the references to color in the figure legend, the reader is referred to the web version of this article.)

where λ_1 and λ_2 are the two eigenvalues of 2×2 structure tensor J and we assume $\lambda_1 \geq \lambda_2$. This quantity of OC can indicate how strongly the energy is concentrated along the ridge orientation. If there is a dominant ridge orientation, then $\lambda_1 \gg \lambda_2$ and OC will be close to 1. Otherwise, λ_1 and λ_2 will not differ much and consequently OC will be close to 0.

We also calculate a measurement related to the intensity contrast (IC) of the block as follows:

$$IC = std(B) \tag{6}$$

where *std* denotes the standard deviation. The purpose of this is to exclude the background from the foreground fingerprint. The two measurements, OC and IC, are evaluated with pre-specified thresholds. If both of them are above the thresholds, the block is recorded as a well-defined block and will not be further partitioned. Otherwise, the block larger than the minimum size is evenly partitioned into four equal sub-blocks, each of which is further examined. Suppose a block has reached the minimum size, this block will be marked as a well-defined block if its OC and IC measures are above the thresholds; it is marked as an ill-posed block if its OC measure is less than the threshold but the IC measure is above the threshold; otherwise, it is marked as a background block. Fig. 5(b) shows the partition result of the image in Fig. 5(a). The dominant ridge orientations of the well-defined blocks are shown by the green lines.

After partitioning the fingerprint image into the three kinds of blocks, the pores can be extracted from each of the foreground (well-defined or ill-posed) blocks. For a well-defined block, the dominant ridge orientation and the mean ridge frequency on it can be calculated directly, and hence the DAPM can be consequently instantiated. For an ill-posed block, there is no dominant ridge orientation but the mean ridge frequency can be calculated by interpolating the mean ridge frequencies of its neighboring blocks. Hence, as a compromise, we apply to the ill-posed blocks the adaptive DoG based pore models [25]. Next we discuss on how to calculate the dominant ridge orientation of a well-defined block and the mean ridge frequency on a foreground block.

The dominant orientation of a well-defined block is defined as the average orientation of the ridge orientation field on the block. To average the orientation field of block B, denoted by B_{OF}, we first multiply the orientation angle at each pixel by 2, and then calculate its cosine and sine values. Finally, the dominant orientation of the block is calculated as

$$B_{DO} = \frac{1}{2}\arctan\left(\frac{aver(\sin(2\bullet B_{OF}))}{aver(\cos(2\bullet B_{OF}))}\right) \tag{7}$$

where $aver(F)$ denotes the average of the elements in F.

For each well-defined block, the average ridge frequency on the block is calculated by using the method in [19]. The ridge frequencies on the ill-posed blocks are estimated by interpolating their surrounding blocks whose ridge frequencies have already been calculated. Specifically, after the ridge frequencies on well-defined blocks have been calculated, we iteratively check the fingerprint image until all the ridge frequencies of the foreground blocks have been calculated. If the ridge frequency of a foreground block has not been calculated, we take the mean of the ridge frequencies of its neighboring blocks as its ridge frequency. Finally, all foreground fingerprint blocks, no matter with or without dominant orientation, are assigned with ridge frequencies.

4.3. The pore extraction algorithm

We now summarize the complete adaptive fingerprint pore extraction algorithm. As shown in Fig. 6, the proposed pore extraction algorithm consists of five main steps. Take the fingerprint fragment in Fig. 7(a), which is a part of Fig. 5(a), as an example. The first step is to partition the fingerprint image into a number of blocks, each being a well-defined block, an ill-posed block or a background block (see Fig. 7(b)). In the second step, the ridge orientation field of the fingerprint image is calculated. Meanwhile, the mean ridge frequencies on all foreground blocks are estimated, which form the ridge frequency map of the fingerprint image (see Fig. 7(c)). It then proceeds to the third step, in which the binary ridge map of the fingerprint image is calculated as follows. Based on the estimated ridge orientation field and ridge frequency map, the fingerprint image is first enhanced by using a bank of Gabor filters [19] to enhance the bright valleys and suppress dark ridges. In order to extract the ridges from the fingerprint image, we binarize the enhanced image and calculate its complement, where the ridge pixels have value '1'. With this complement image, we can readily obtain the binary ridge map by setting the corresponding ridge pixels in the foreground fingerprint blocks to '1' and the other pixels to '0'. This binary ridge map (see Fig. 7(d)) will be used in the post-processing step to remove spurious pores because pores can only locate on ridges.

It is worth mentioning that the first three steps can be performed on a down-sampled small image of the original high resolution fingerprint image because they do not depend on the Level 3 features. In our experiments, we down-sampled the images to half of their original resolution and then carried out steps A, B, and C. Afterwards, the obtained image partition result, ridge orientation field, ridge frequency map, and the ridge map

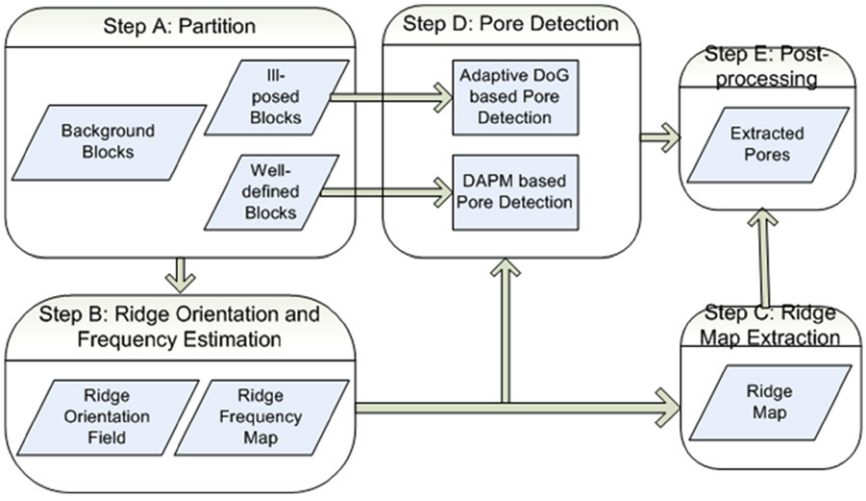

Fig. 6. The main steps of the proposed pore extraction method.

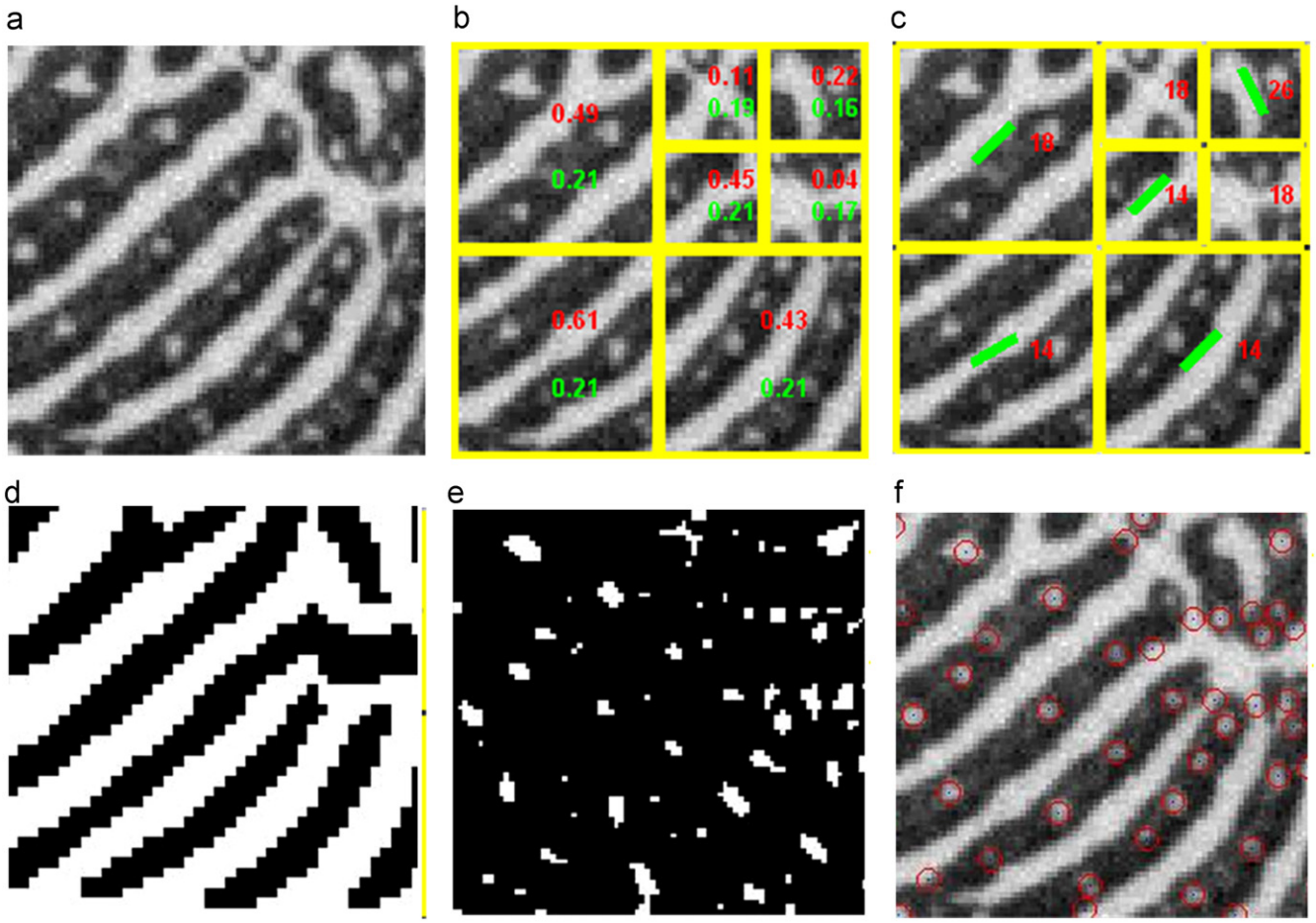

Fig. 7. (a) Is a fingerprint fragment, (b) shows the blocks on it (the value in red is the orientation certainty and the value in green is the intensity contrast), (c) displays the estimated dominant ridge orientations and periods (the green lines denote the orientations on well-defined blocks, and if there is no orientation shown on a block, the block is an ill-posed block), (d) is the ridge map, (e) is the initial pore map, and (f) shows the final detected pores (marked by circles). (For interpretation of the references to color in the figure legend, the reader is referred to the web version of this article.)

were all up-sampled to the original resolution. They will be used in the subsequent pore detection and post-processing. Working on the down-sampled images can reduce a lot of computational cost. The pore detection and post-processing are performed on the original fingerprint images because the Level 3 pore features can hardly be reliably extracted in the down-sampled low resolution fingerprint images.

In the pore detection step, the foreground fingerprint blocks are processed one by one to detect pores on them. A local instantiation of the DAPM is established for each well-defined block based on the local ridge orientation and frequency on that block, and a local instantiation of the adaptive DoG based pore model is established for each ill-posed block based on the local ridge frequency on the block. Applying the adaptively instantiated pore model to the block as a matched filter will enhance the pores while suppressing valleys and noise. A threshold is then applied to the filtering response to segment out the candidate pores on the block. After processing all the blocks, we obtain a binary image where the candidate pores have the value '1' and other pixels have value '0'. This binary image gives the initial pore extraction result (pore map). Fig. 7(e) shows an example. We can see that there could have some spurious and false pores in this map.

The last step is to remove the spurious and false pores from the initial pore extraction result. In previous work, most methods remove false pores by applying the restraint that pores should reside only on ridges [10–12,14] and that the size of pores should be within a valid range [10–11,14]. Some researchers also propose to refine the pore extraction result based on the intensity contrast [13]. In [13], a PCA method is applied to a set of extracted putative pores to estimate a model for the gray level distribution over pores. This model is then used to exclude falsely detected pores based on a method of minimizing squared error. This method is however greatly affected by the chosen putative pores.

In this paper, we take the following steps to post-process the extracted candidate pores. First, we use the binary ridge map as a mask to filter the pore map. In this step, the pixels which are not on ridges are removed. Second, we sort the remaining candidate pore pixels according to their gray level values descendingly and then discard the last 5% pixels because they are more probably caused by noise. Third, we identify all the connected components on the pore map, and each component is taken as a candidate pore. We check the size of each component, i.e. the number of pixels it has. If the size is out of the pre-specified range of valid pore size (from 3 to 30 in our experiments), the candidate pore is removed from the pore map. The final pore map is obtained after the above refinement. We record the extracted pores by recording the coordinates of their mass centers. See Fig. 7(f) for an example. More examples of different fingerprint fragments are given in Fig. 8.

5. Experiments and performance evaluation

To evaluate the proposed fingerprint pore extraction method, a high resolution fingerprint image dataset is required. It is well

accepted that the fingerprint image resolution should be at least 1000 dpi to reliably capture the Level 3 features such as pores [5]. Unfortunately, so far there is no such high resolution fingerprint image database freely available in the public domain. So we built an optical fingerprint scanner by ourselves, which could collect the fingerprint images at a resolution of about 1200 dpi. Fig. 9 shows the scanner we developed. It uses a CCD camera (Lumenera Camera LU135M) to capture the fingerprint image when the finger touches against the prism of the scanner.

Two databases have been established by using the scanner we developed. The first database (denoted as DBI) is a partial fingerprint image database where the image size is 320 pixels in width and 240 pixels in height. The second database (denoted as DBII) contains full-size fingerprint images which are 640 pixels in width and 480 pixels in height. Both databases have 1480 fingerprint images taken from 148 fingers with each finger having 10 samples in two sessions. Five images were captured for each finger in each of the two sessions which were about two weeks apart.

Using the established databases, we have conducted extensive experiments to evaluate the proposed pore extraction method in comparison with three state-of-the-art methods (Jain's method [10,11], Ray's method [12], and the adaptive DoG based method [25]). Three types of experiments were conducted. First, we compared the proposed method with its counterparts in terms of pore detection accuracy using a set of fingerprint images chosen from DBI. Second, using the partial fingerprint image database DBI and a minutia-pore-based fingerprint matcher, we evaluated the fingerprint recognition performance by using the pores extracted by the proposed method and the other three methods. Third, we evaluated the fingerprint recognition performance of the four methods on the full-size fingerprint image database DBII. In the following, we present the experiments in detail.

5.1. Pore detection accuracy

We first assess the pore detection accuracy of the proposed method. For this purpose, we chose a set of 24 fingerprint images from DBI. The chosen images have relatively good quality so that the pores on them can be easily marked. Fig. 10 shows two

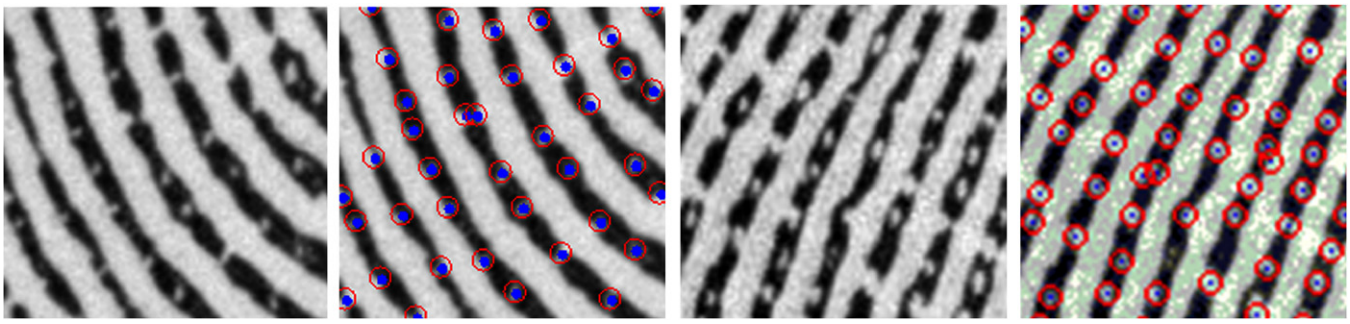

Fig. 8. Some example pore extraction results obtained by using the proposed method.

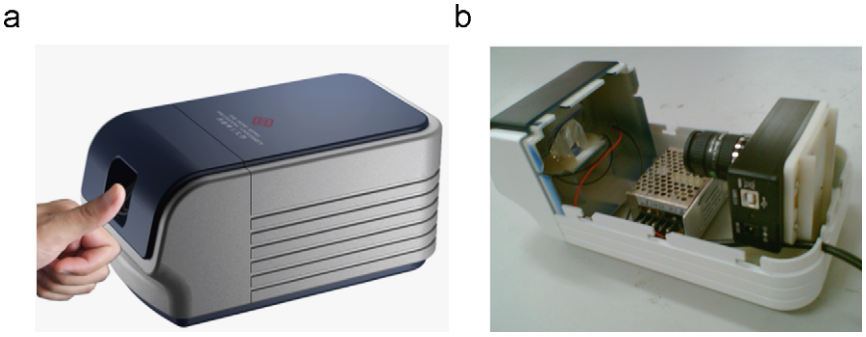

Fig. 9. (a) The high-resolution fingerprint scanner we developed and (b) its inner structure.

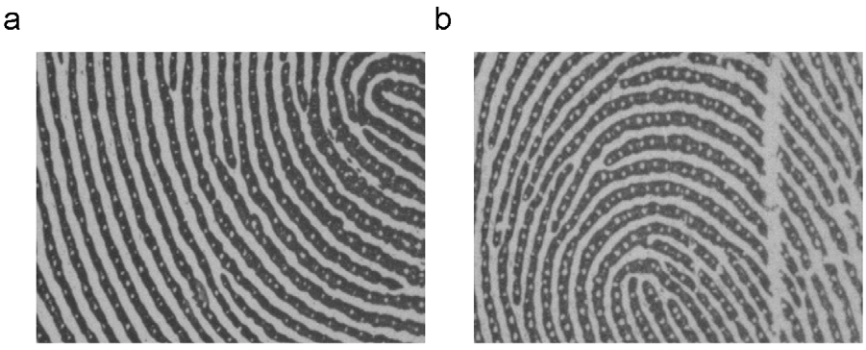

Fig. 10. Two example fingerprint images used in the experiments.

example fingerprint images. We manually marked the pores on these fingerprint images as the ground truth for our experiments. We then used our proposed method, Jain's method, Ray's method, and the adaptive DoG based method to extract pores on them. Fig. 11 shows the pore extraction results of the four methods on the fingerprint image in Fig. 10(b). On this fingerprint fragment, the ridges on the left hand side are thinner than those on the right hand side, and both open and closed pores can be observed. From Fig. 11(a) and (b), we can see that due to the unitary scale they use, Ray's method and Jain's method cannot work consistently well on the left and the right parts of the fingerprint image because of the varying ridge widths and pore sizes. In addition, all the three comparison methods miss many open pores because their isotropic pore models cannot accurately handle open pores. In contrast, the proposed method successfully detects most of the pores on both the left and the right parts of the fingerprint image no matter they are open or closed. This demonstrates that the proposed DAPM model can better adapt to varying ridge widths and pore sizes, and can better cope with both closed and open pores.

In addition to the visual evaluation of the pore detection results, we calculated the average detection accuracy on the 24 fingerprint images by using two metrics: R_T (true detection rate) and R_F (false detection rate). R_T is defined as the ratio of the number of detected true pores to the number of all true pores, while R_F is defined as the ratio of the number of falsely detected pores to the total number of detected pores. A good pore extraction algorithm should have a high R_T and a low R_F simultaneously. Table 1 lists the average detection accuracy and the standard deviation of detection accuracy of the four methods. According to the average detection accuracy listed in Table 1, the proposed method achieves not only the highest true detection rate but also the lowest false detection rate. With regard to the standard deviation, as shown in Table 1, the proposed method again achieves the smallest deviation over the whole image set for both true detection rate and false detection rate. As for the other three methods, none beats its counterparts in all cases. From these results, we can see that the proposed method can detect pores on fingerprint images more accurately and more robustly.

5.2. Pore based partial-fingerprint recognition

Since the purpose of pore extraction is to introduce new features for fingerprint recognition, it is necessary to test how the pores extracted by the methods will contribute to a fingerprint recognition system. According to [8,9,26], the fingerprint recognition benefits more from the pores when the used fingerprint images cover small fingerprint area. Therefore, in order to emphasize the contribution of pores, we evaluated in this subsection the improvement of fingerprint recognition accuracy made by the extracted pores based on the partial fingerprint image database DBI.

We implemented an AFRS like the one in [26] which is based on minutiae and pores. The block diagram of the AFRS is shown in Fig. 12. It consists of five main modules, i.e. minutia extraction, pore extraction, minutia matching, pore matching, and match

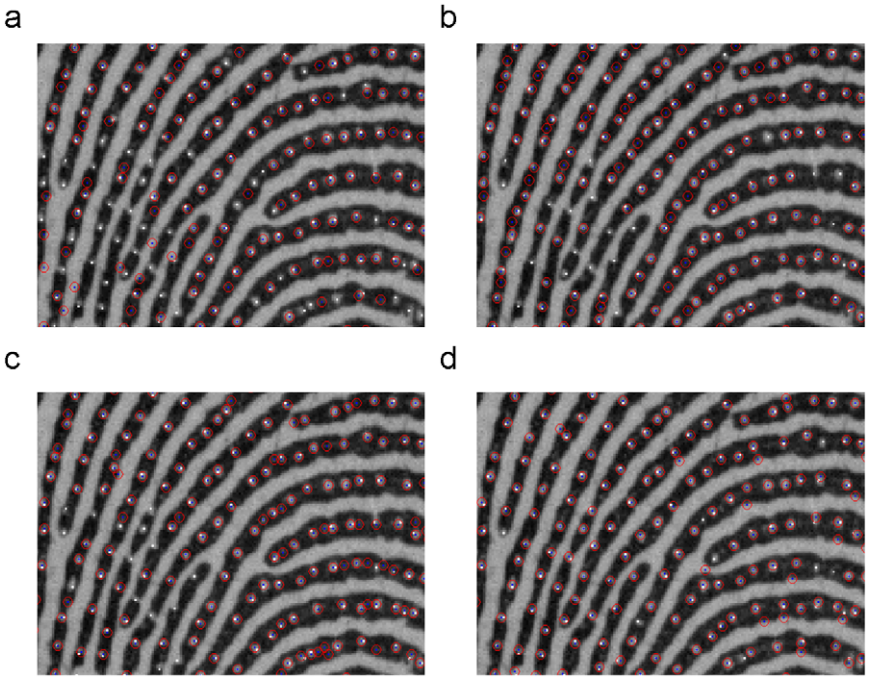

Fig. 11. Example pore extraction results of (a) Ray's method, (b) Jain's method, (c) the adaptive DoG based method, and (d) the proposed method. The pores are manually marked by bright dots and the detected pores are marked by red circles. (For interpretation of the references to color in the figure legend, the reader is referred to the web version of this article.)

Table 1
The average pore detection accuracy (%) and the standard deviation of the four methods on the 24 fingerprint images.

	Ray's method	Jain's method	Adaptive DoG based method	The proposed method
R_T	60.6 (11.9)	75.9 (7.5)	80.8 (6.5)	84.8 (4.5)
R_F	30.5 (10.9)	23.0 (8.2)	22.2 (9.0)	17.6 (6.3)

score fusion. We use the methods in [21] for minutia extraction and matching modules. The pore matching is accomplished by using the direct pore matching method in [26]. It firstly establishes initial correspondences between the pores on two fingerprints based on their local features, and then uses the RANSAC (Random Sample Consensus) algorithm [27] to refine the pore correspondences, and finally calculates a pore-based similarity score between the two fingerprints based on the number of corresponding pores. The pore matching is independent of minutia matching in this method. This method is very suitable for small partial fingerprint recognition where the minutia matching results are often unreliable due to the limited number of minutiae on the small fingerprint fragments [26]. The pore match score and the minutia match score are finally fused by using a simple weighted summation scheme to give the final match score between two fingerprint images (before fusion, both match scores are normalized to the range between 0 and 1) as follows:

$$MS = \omega MS_{\text{minu}} + (1-\omega) MS_{\text{pore}} \tag{8}$$

where ω is the weight of minutiae with respect to pores.

By using database DBI and the above described AFRS, we evaluated the fingerprint recognition performance of the four pore extraction methods. Considering the expensive computational cost, the following matches were carried out: (1) Genuine matches: Each of the fingerprint images in the second session was matched with all the fingerprint images in the first session, leading to 3700 genuine matches, and (2) Imposter matches: the first fingerprint image of each finger in the second session was matched with the first fingerprint image of all the other fingers in the first session, resulting in 21,756 imposter matches. Fig. 13 shows the equal error rates (EER) obtained by the four methods on DBI under different weights. By using only minutiae, the EER is 17.67%. The EERs when using only pores (i.e. $\omega=0$) are, respectively, 21.96% by Ray's method, 21.53% by Jain's method, 22.99% by the adaptive DoG

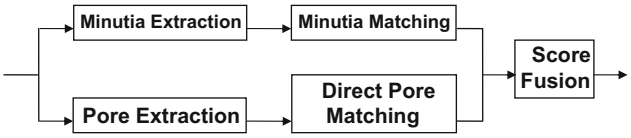

Fig. 12. Block diagram of the AFRS used in partial fingerprint recognition experiments.

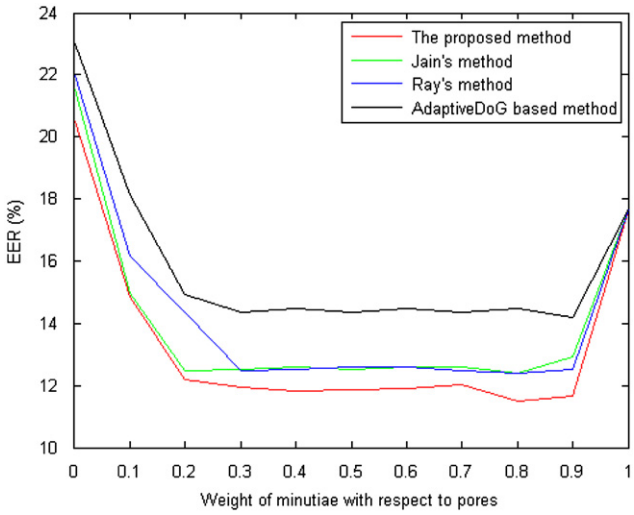

Fig. 13. The EERs of the four methods on DBI with different fusing weights.

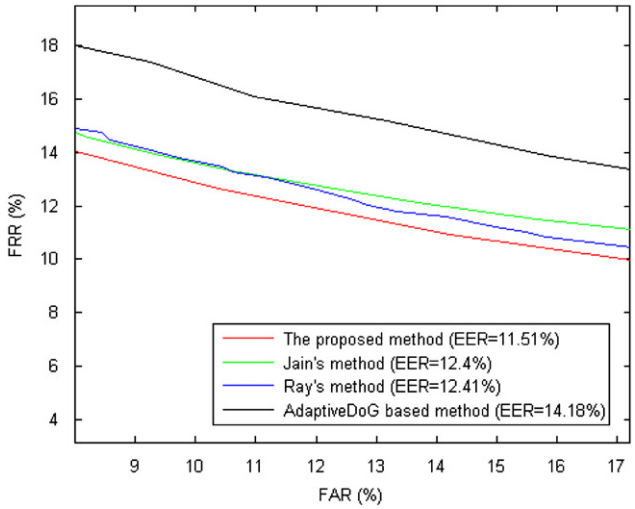

Fig. 14. The ROC curves of the four methods on DBI when the lowest EERs are obtained.

based method, and 20.49% by the proposed method. By fusing minutiae and pores, the best results are 12.41% ($\omega=0.9$), 12.4% ($\omega=0.8$), 14.18% ($\omega=0.9$), and 11.51% ($\omega=0.8$) by the four methods, respectively. Fig. 14 shows their receiver operating characteristics (ROC) curves when the best EERs are obtained. It is seen that the proposed method leads to the best recognition results. The improvement of recognition accuracy made by fusing the pore features over using only minutia features are 29.77%, 29.82%, 19.75% and 34.86%, respectively by the four methods.

5.3. Pore based full-size fingerprint recognition

The experiments in this sub-section were to evaluate the contribution of the extracted pores to full-size fingerprint recognition. We compared the four pore extraction methods by using a different AFRS in [10], which is appropriate for full-size fingerprint images, and using the full-size fingerprint image database DBII. Fig. 15 shows the block diagram of the AFRS. We used the same minutia extraction and matching modules and the same score fusion module as in the last sub-section, but implemented the pore matching module by using the ICP (iterative closest point) based method as in [10,11]. This is because on fingerprint images covering large fingerprint area, there are sufficient minutiae to provide reliable minutia match results. We can thus compare the pores locally in the neighborhoods of matched minutiae. In this way, the pores can be matched much more efficiently. Specifically, after matching the minutiae on two fingerprints, the pores lying in the neighborhoods of each pair of matched minutiae are matched by using the ICP algorithm [10,11], resulting in N match scores (N is the number of pairs of matched minutiae), which are defined as the summation of two terms: the mean distance between all matched pores and the percentage of unmatched pores. The pore match score between the two fingerprints is finally defined as the average of the first three smallest match scores.

By using the above AFRS, we matched pair-wise all the fingerprint images in DBII (avoiding symmetric matches), generating 6660 genuine match scores and 1,087,800 imposter match scores. Fig. 16 presents the EERs obtained by the four methods on DBII. Because the fingerprint images in DBII are full-size fingerprint images and have more minutiae, it can be seen that the EER of using only minutiae is 0.61%, which is much better than that obtained on DBI (17.67%, referring to Section 5.2). When only using pores, the EER of Ray's method is 9.45%, Jain's method 8.82%, the adaptive DoG based method 10.85%, and the proposed method

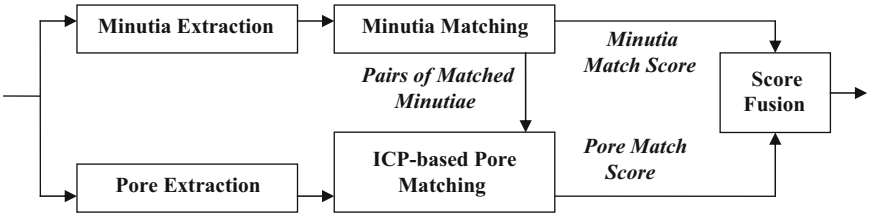

Fig. 15. Block diagram of the AFRS used in full-size fingerprint recognition experiments.

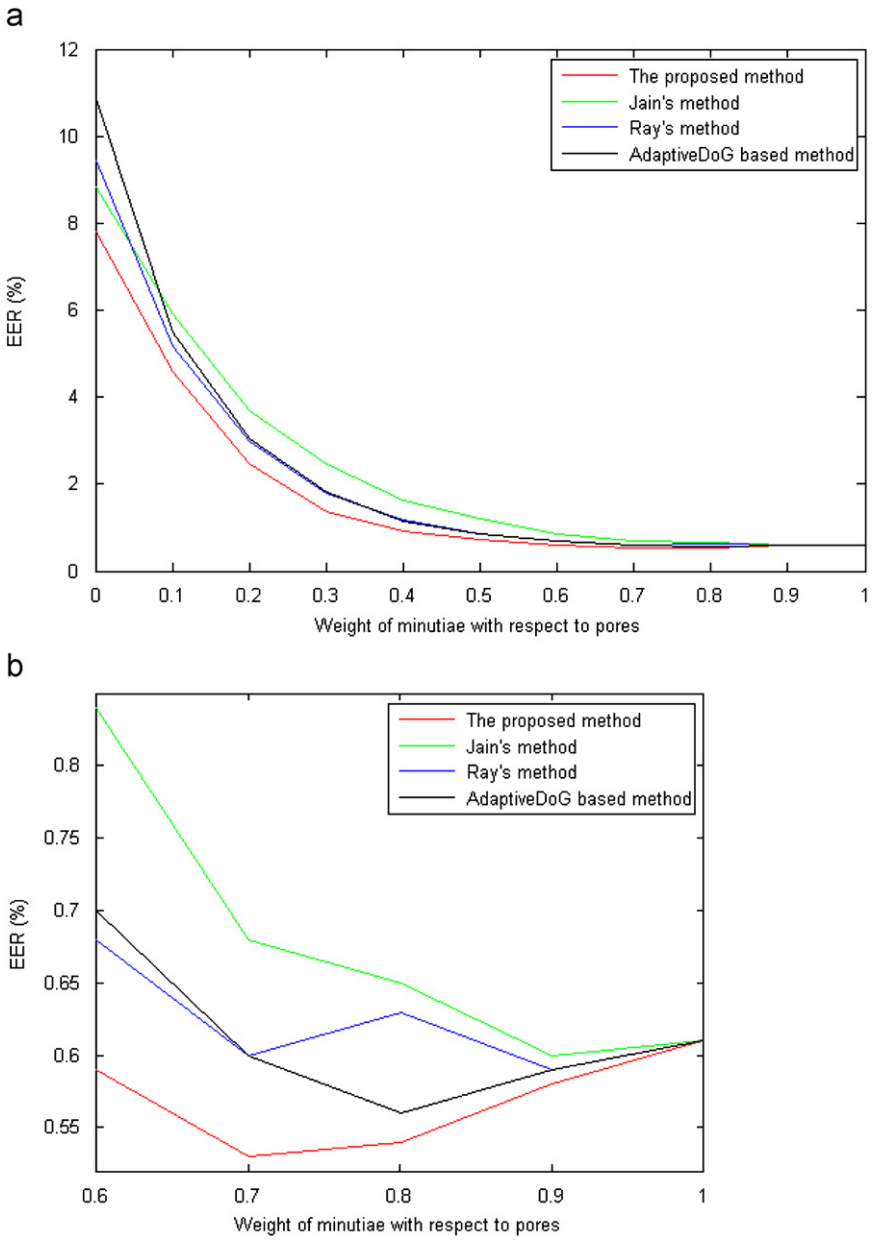

Fig. 16. The EERs of the four methods on DBII when different weights are used. (b) is the zoom-in of (a) when the weight is from 0.6 to 1.

7.81%. The best results of these methods after fusion with minutia match scores are 0.59% ($\omega=0.9$), 0.6% ($\omega=0.9$), 0.56%($\omega=0.8$), and 0.53% ($\omega=0.7$). Fig. 17 shows their corresponding ROC curves when the best results are obtained. The proposed method improves on the best EERs of Ray's method, Jain's method, and the adaptive DoG based method by 10.17%, 11.67%, and 5.36%, respectively.

5.4. Computational complexity analysis

Before closing this section, we would like to briefly analyse the computational complexity of the methods. As shown in Fig. 6, the proposed pore extraction method has five main steps: (A) partition, (B) ridge orientation and frequency estimation, (C) ridge

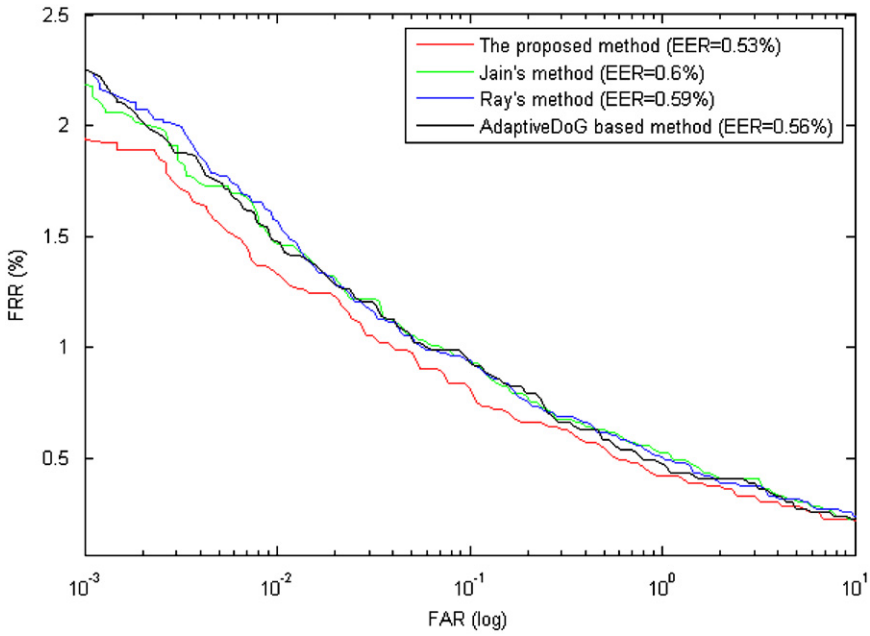

Fig. 17. The ROC curves of the four methods on DBII when the best results are obtained.

map extraction, (D) pore detection, and (E) post-processing. Among these steps, the steps (B) and (C) are common to most automatic fingerprint recognition systems. The step (A) needs to calculate the two measurements, *OC* and *IC*, for each of the blocks, which can be done very efficiently. On a PC with 2.13 GHz Intel(R) Core(TM) 2 6400 CPU and RAM of 2 GB, the Matlab implementation of the method took about 0.05 ms on average to conduct the step (*A*) for one partial fingerprint image used in the experiments (note that down-sampling was applied in the experiments). In the pore detection step (*D*), the main operation is the convolution of pore models with the fingerprint image. This is essentially common to all filtering-based pore extraction methods including the three counterpart methods considered in the experiments here. However, because Jain's and Ray's methods both apply a single pore filter to the whole fingerprint image, they are more efficient than the Adaptive DoG-based method and the method proposed here which apply different pore filters to different blocks. Specifically, Jain's and Ray's methods took less than 0.1 ms to detect the pores on one partial fingerprint image, whereas the other two methods used about 0.5 ms. The last post-processing step (*E*) is also common to all pore extraction methods. Using our Matlab implementation, it took about 0.4 ms to carry out all the post-processing operations defined in Section 4.3. From the above analysis, we can see that the proposed pore extraction method is a little more complex than Jain's and Ray's methods due to the more elaborated pore models on which it is based. However, considering the gain of accuracy by the proposed method, the increased computational complexity is deserved. More importantly, its computational cost is still acceptable (with the Matlab implementation, it took about 1–2 s to extract the pores on one partial fingerprint image), and we expect that the computational cost can be much reduced by using languages like C/C++ and after optimization.

6. Conclusion

This paper presented a dynamic anisotropic pore model (DAPM). It differs from previous pore models in that it is anisotropic and dynamic so that it can more accurately represent pores by using orientation and scale parameters. A novel adaptive pore extraction method was then developed based on the DAPM. The fingerprint image was partitioned into well-defined, ill-posed and background blocks according to the orientation certainty and intensity contrast on the blocks. For each well-defined block, the ridge orientation and frequency were estimated directly, while for each ill-posed block, the ridge frequency was estimated by interpolating the ridge frequencies on its neighboring blocks. The local instances of the DAPM were then instantiated for the well-defined blocks based on the estimated orientations and frequencies of them. The instantiated pore models were taken as the matched filters and applied to the blocks to detect the pores thereon. In the post-processing step, some constraints were used to remove possible spurious and false pores in the detection result.

We have established two high-resolution fingerprint databases to evaluate the proposed method in comparison with three state-of-the-art pore extraction methods. The proposed method obtained a true detection rate as 84.8% and a false detection rate as 17.6%, and corresponding deviations 4.5% and 6.3%. In contrast, the best true detection rate and false detection rate of existing methods were, respectively, 80.8% and 22.2%, and their deviations were 6.5% and 8.2%. These experimental results demonstrated that the proposed DAPM is more accurate and robust than the previous models. We consequently evaluated the pore based fingerprint recognition systems. The experiments show that by using pores as additional features to the conventional minutia features, higher recognition accuracy can be obtained. Since the proposed DAPM achieves higher pore detection accuracy, it obtains the best fingerprint recognition accuracy among the state-of-the-art pore extraction methods on both partial and full-size fingerprint image databases. On the partial fingerprint image database, by fusing minutia and pore match scores it improves the recognition accuracy of using only minutiae by 34.86%, whereas the improvements made by the other methods are all below 30%. On the full-size fingerprint image database, again, the proposed method achieves the best EER at 0.53%, which improves the other methods by over 5% to about 12%.

In this paper, we experimentally set the scale parameter of the proposed pore model according to the local ridge periods by a ratio. In our future work, we are going to determine it in a more adaptive way based on the automatic scale selection theory [17,28]. Currently, the proposed pore extraction method is mainly

for live-scan fingerprints. In future, we are also going to extend the proposed method to more challenging latent fingerprints.

Acknowledgements

The authors would like to thank the editor and the anonymous reviewers for their help in improving the paper. The work is partially supported by the GRF fund from the HKSAR Government, the central fund from Hong Kong Polytechnic University, and the NSFC fund (No. 60803090), the Natural Scientific Research Innovation Foundation in Harbin Institute of Technology, and the Shenzhen Key Laboratory of Network Oriented Intelligent Computation, China.

References

[1] D. Zhang, Automated Biometrics: Technologies and Systems, Kluwer and Academic Publishers, USA, 2000.
[2] A.K. Jain, P. Flynn, A. Ross, Handbook of Biometrics, Springer, 2007.
[3] D. Maltoni, D. Maio, A.K. Jain, S. Prabhakar, Handbook of Fingerprint Recognition, Springer, New York, 2003.
[4] N. Ratha, R. Bolle, Automatic Fingerprint Recognition Systems, Springer, New York, 2004.
[5] CDEFFS, Data format for the interchange of extended fingerprint and palmprint features, Working Draft Version 0.4, 〈http://fingerprint.nist.gov/standard/cdeffs/index.html〉, June 2009.
[6] A. Roddy, J. Stosz, Fingerprint features – statistical analysis and system performance estimates, Proceedings of the IEEE 85 (9) (1997) 1390–1421.
[7] J.D. Stosz, L.A. Alyea, Automated system for fingerprint authentication using pores and ridge structure, in: Proceedings of the SPIE Conference on Automatic Systems for the Identification and Inspection of Humans, San Diego, vol. 2277, 1994, pp. 210–223.
[8] K. Kryszczuk, A. Drygajlo, P. Morier, Extraction of level 2 and level 3 features for fragmentary fingerprints, in: Proceedings of the 2nd COST Action 275 Workshop, 2004, pp. 83–88.
[9] K. Kryszczuk, P. Morier, A. Drygajlo, Study of the distinctiveness of level 2 and level 3 features in fragmentary fingerprint comparison, in: BioAW2004, LNCS 3087, 2004, pp. 124–133.
[10] A.K. Jain, Y. Chen, M. Demirkus, Pores and ridges: Fingerprint matching using level 3 features, in: Proceedings of ICPR06, vol. 4, 2006, pp. 477–480.
[11] A.K. Jain, Y. Chen, M. Demirkus, Pores and ridges: fingerprint matching using level 3 features, IEEE Transactions on Pattern Analysis and Machine Intelligence 29 (1) (2007) 15–27.
[12] M. Ray, P. Meenen, R. Adhami, A novel approach to fingerprint pore extraction, in: Proceedings of the 37th South-eastern Symposium on System Theory, 2005, pp. 282–286.
[13] N.R. Parsons, J.Q. Smith, E. Thonnes, L. Wang, R.G. Wilson, Rotationally invariant statistics for examining the evidence from the pores in fingerprints, Law, Probability and Risk 7 (2008) 1–14.
[14] N. Ratha, K. Karu, S. Chen, A.K. Jain, A real-time matching system for large fingerprint databases, IEEE Transactions on Pattern Analysis and Machine Intelligence 18 (8) (1996) 799–813.
[15] D.R. Ashbaugh, Quantitative–Qualitative Friction Ridge Analysis: An Introduction to Basic and Advanced Ridgeology, CRC Press LLC, 1999.
[16] B. Bindra, O.P. Jasuja, A.K. Singla, Poroscopy: a method of personal identification revisited, Internet Journal of Forensic Medicine and Toxicology 1 (1) (2000).
[17] M. Sofka, C.V. Stewart, Retinal vessel centerline extraction using multiscale matched filters, confidence and edge measures, IEEE Transactions on Medical Imaging 25 (12) (2006) 1531–1546.
[18] A.M. Bazen, S.H. Gerez, Systematic methods for the computation of the directional fields and singular points of fingerprints, IEEE Transactions on Pattern Analysis and Machine Intelligence 24 (7) (2002) 905–919.
[19] L. Hong, Y. Wan, A.K. Jain, Fingerprint image enhancement: algorithms and performance evaluation, IEEE Transactions on Pattern Analysis and Machine Intelligence 20 (8) (1998) 777–789.
[20] Y. Chen, S. Dass, A. Jain, Fingerprint quality indices for predicting authentication performance, in: Proceedings of AVBPA2005, 2005, pp. 160–170.
[21] J. Feng, Combining minutiae descriptors for fingerprint matching, Pattern Recognition 41 (2008) 342–352.
[22] A. Ross, A. Jain, J. Reisman, A hybrid fingerprint matcher, Pattern Recognition 36 (2003) 1661–1673.
[23] A. Jain, L. Hong, R. Bolle, On-line fingerprint verification, IEEE Transactions on Pattern Recognition and Machine Intelligence 19 (4) (1997) 302–314.
[24] Y. He, J. Tian, L. Li, H. Chen, X. Yang, Fingerprint matching based on global comprehensive similarity, IEEE Transactions on Pattern Analysis and Machine Intelligence 28 (6) (2006) 850–862.
[25] Q. Zhao, D. Zhang, L. Zhang, N. Luo, High resolution partial fingerprint alignment using pore-valley descriptors, Pattern Recognition 43 (3) (2010) 1050–1061.
[26] Q. Zhao, L. Zhang, D. Zhang, N. Luo, Direct pore matching for fingerprint recognition, in: Proceedings of ICB2009, 2009, pp. 597–606.
[27] R. Hartley, A. Zisserman, Multiple View Geometry in Computer Vision, 2nd ed, Cambridge University, 2003.
[28] T. Lindeberg, Edge detection and ridge detection with automatic scale section, International Journal of Computer Vision 30 (1998) 117–156.

About the Author—QIJUN ZHAO holds a B.S. degree and an M.S. degree both from the Department of Computer Science and Engineering, Shanghai Jiao Tong University, Shanghai, China. He received his Ph.D. degree in computer science from the Department of Computing at the Hong Kong Polytechnic University in 2010. He is now a post-doc fellow in the Pattern Recognition and Image Processing Lab at Michigan State University. His research interests mainly lie in the fields of pattern recognition, machine learning, image processing, and artificial intelligence, with applications to biometrics, information security, and intelligent systems.

About the Author—DAVID ZHANG graduated in Computer Science from Peking University. He received his M.Sc. in Computer Science in 1982 and his Ph.D. in 1985 from the Harbin Institute of Technology (HIT). From 1986 to 1988 he was a Postdoctoral Fellow at Tsinghua University and then an Associate Professor at the Academia Sinica, Beijing. In 1994 he received his second Ph.D. in Electrical and Computer Engineering from the University of Waterloo, Ontario, Canada. Currently, he is a Head, Department of Computing, and a Chair Professor at the Hong Kong Polytechnic University where he is the Founding Director of the Biometrics Technology Centre (UGC/CRC) supported by the Hong Kong SAR Government in 1998. He also serves as Visiting Chair Professor in Tsinghua University, and Adjunct Professor in Peking University, Shanghai Jiao Tong University, HIT, and the University of Waterloo. He is the Founder and Editor-in-Chief, International Journal of Image and Graphics (IJIG); Book Editor, Springer International Series on Biometrics (KISB); Organizer, the International Conference on Biometrics Authentication (ICBA); Associate Editor of more than 10 international journals including IEEE Transactions and Pattern Recognition; Technical Committee Chair of IEEE CIS and the author of more than 10 books and 200 journal papers. Professor Zhang is a Croucher Senior Research Fellow, Distinguished Speaker of the IEEE Computer Society, and a Fellow of both IEEE and IAPR.

About the Author—LEI ZHANG received the B.S. degree in 1995 from Shenyang Institute of Aeronautical Engineering, Shenyang, P.R. China, the M.S. and Ph.D. degrees in Electrical and Engineering from Northwestern Polytechnical University, Xi'an, P.R. China, respectively in 1998 and 2001. From 2001 to 2002, he was a research associate in the Dept. of Computing, The Hong Kong Polytechnic University. From January 2003 to January 2006 he worked as a Postdoctoral Fellow in the Dept. of Electrical and Computer Engineering, McMaster University, Canada. Since Jan. 2006, he has been an Assistant Professor in the Dept. of Computing, The Hong Kong Polytechnic University. His research interests include Image and Video Processing, Biometrics, Pattern Recognition, Computer Vision, Multisensor Data Fusion and Optimal Estimation Theory, etc.

About the Author—NAN LUO received the B.S. degree in 2003 and he is now working as a Research Assistant at the Biometrics Research Centre of the Hong Kong Polytechnic University. His research interests include imaging technology and biometric systems.